

See discussions, stats, and author profiles for this publication at: <https://www.researchgate.net/publication/6701511>

# Identification and regional distribution in rat brain of radiometabolites of the dopamine transporter PET radioligand [C-11]PE2I

ARTICLE *in* EUROPEAN JOURNAL OF NUCLEAR MEDICINE AND MOLECULAR IMAGING · JUNE 2007

Impact Factor: 5.38 · DOI: 10.1007/s00259-006-0277-1 · Source: PubMed

CITATIONS

44

READS

24

10 AUTHORS, INCLUDING:



**H. Umesha Shetty**

U.S. Department of Health and Human Ser...

63 PUBLICATIONS 1,482 CITATIONS

SEE PROFILE



**Sami S Zoghbi**

National Institutes of Health

298 PUBLICATIONS 10,393 CITATIONS

SEE PROFILE



**Jinsoo Hong**

U.S. Department of Health and Human Ser...

71 PUBLICATIONS 1,448 CITATIONS

SEE PROFILE



**Victor Pike**

National Institutes of Health

444 PUBLICATIONS 9,423 CITATIONS

SEE PROFILE

# Identification and regional distribution in rat brain of radiometabolites of the dopamine transporter PET radioligand [ $^{11}\text{C}$ ]PE2I

H. Umesha Shetty · Sami S. Zoghbi · Jieih-San Liow · Masanori Ichise · Jinsoo Hong · John L. Musachio · Christer Halldin · Jurgen Seidel · Robert B. Innis · Victor W. Pike

Received: 3 March 2006 / Accepted: 2 September 2006 / Published online: 10 November 2006  
© Springer-Verlag 2006

## Abstract

**Purpose** We aimed to determine the composition of radioactivity in rat brain after intravenous administration of the dopamine transporter radioligand, [ $^{11}\text{C}$ ]PE2I.

**Methods** PET time-activity curves (TACs) and regional brain distribution ex vivo were measured using no-carrier-added [ $^{11}\text{C}$ ]PE2I. Carrier-added [ $^{11}\text{C}$ ]PE2I was administered to identify metabolites with high-performance liquid radiochromatography (RC) or RC with mass spectrometry (LC-MS and MS-MS). The stability of [ $^{11}\text{C}$ ]PE2I was assessed in rat brain homogenates.

**Results** After peak brain uptake of no-carrier-added [ $^{11}\text{C}$ ]PE2I, there was differential washout rate from striata and cerebellum. Thirty minutes after injection, [ $^{11}\text{C}$ ]PE2I represented  $10.9 \pm 2.9\%$  of the radioactivity in plasma,  $67.1 \pm 11.0\%$  in cerebellum, and  $92.5 \pm 3.2\%$  in striata, and was accompanied by two less lipophilic radiometabolites. [ $^{11}\text{C}$ ]PE2I was stable in rat brain homogenate for at least

1 h at 37°C. LC-MS identified hydroxylated PE2I (**1**) ( $m/z$  442) and carboxyl-desmethyl-PE2I (**2**) ( $m/z$  456) in brain. MS-MS of **1** gave an  $m/z$  442→424 transition due to  $\text{H}_2\text{O}$  elimination, so verifying the presence of a benzyl alcohol group. Metabolite **2** was the benzoic acid derivative. Ratios of ex vivo measurements of [ $^{11}\text{C}$ ]PE2I, [ $^{11}\text{C}$ ]**1**, and [ $^{11}\text{C}$ ]**2** in striata to their cognates in cerebellum were  $6.1 \pm 3.4$ ,  $3.7 \pm 2.2$  and  $1.33 \pm 0.38$ , respectively, showing binding selectivity of metabolite [ $^{11}\text{C}$ ]**1** to striata. **Conclusion** Radiometabolites [ $^{11}\text{C}$ ]**1** and [ $^{11}\text{C}$ ]**2** were characterized as the 4-hydroxymethyl and 4-carboxyl analogs of [ $^{11}\text{C}$ ]PE2I, respectively. The presence of the pharmacologically active [ $^{11}\text{C}$ ]**1** and the inactive [ $^{11}\text{C}$ ]**2** is a serious impediment to successful biomathematical analysis.

**Keywords** Dopamine transporter · Brain · PET · [ $^{11}\text{C}$ ]PE2I · Metabolites

H. U. Shetty (✉) · S. S. Zoghbi · J.-S. Liow · M. Ichise · J. Hong · J. L. Musachio · R. B. Innis · V. W. Pike  
PET Radiopharmaceutical Sciences, Molecular Imaging Branch,  
National Institute of Mental Health, National Institutes of Health,  
Building 10, Room B3 C351, MSC 1003, 10 Center Drive,  
Bethesda, MD 20892-1003, USA  
e-mail: shettyu@mail.nih.gov

C. Halldin  
Department of Clinical Neuroscience, Psychiatry Section,  
Karolinska Hospital,  
Stockholm, Sweden

J. Seidel  
Department of Nuclear Medicine, Warren Grant Magnuson  
Clinical Center, National Institutes of Health,  
Bethesda, MD, USA

## Introduction

Methods for measuring dopamine transporter (DAT) density in brain with positron emission tomography (PET) or single-photon emission computed tomography (SPECT) permit noninvasive monitoring of the pathophysiology of Parkinson's disease [1–3], depression [4], schizophrenia [5], and other neurological disorders [6] where impaired activity of dopaminergic neurons is implicated. Several selective and high-affinity radioligands, derived from cocaine, have been evaluated for DAT-specific binding and for PET or SPECT imaging [7–14]. Promising radioligands have emerged from these studies, such as [ $^{18}\text{F}$ ](2 $\beta$ -carbomethoxy-3 $\beta$ -(4-chlorophenyl)-8-(2-fluoroethyl)nortropane

( $[^{18}\text{F}]\text{FECNT}$ ), which has a favorable time course to attain binding equilibrium [10, 14]. However, in a rat model of Parkinson's disease, PET measurements of DAT with  $[^{18}\text{F}]\text{FECNT}$  were confounded by brain accumulation of a polar radiometabolite [15] arising from *N*-dealkylation [16].

*N*-(3-Iodoprop-2*E*-enyl)-2 $\beta$ -carbomethoxy-3 $\beta$ -(4-methylphenyl)nortropine (PE2I; Fig. 1) has been identified as a selective high-affinity DAT ligand ( $K_i=17$  nM) [7]. As a SPECT radioligand,  $^{123}\text{I}$ -labeled PE2I gave high specific to nonspecific uptake ratios in monkey and human brain [8, 17]. Similarly, as a PET radioligand,  $^{11}\text{C}$ -labeled PE2I (Fig. 1) showed high target to nontarget ratios in both human and nonhuman primates [18]. This radioligand has now been subjected to biomathematical interpretation and has entered clinical investigations [19, 20].  $[^{11}\text{C}]\text{PE2I}$  appeared to be a good candidate for PET studies in rat models designed to monitor the efficacy of new therapies in Parkinson's disease [15]. However, initial analysis of regional rat brain PET data has indicated dynamic inconsistencies characteristic of heterogeneity in brain radioactivity [21]. Based on the generally known actions of metabolizing enzymes on diverse classes of drugs and other xenobiotics [22–25], PE2I is expected to undergo phase I metabolism mostly involving benzylic hydroxylation and *N*-dealkylation by cytochrome P450 enzymes and hydrolysis by esterases (Fig. 1). Using this basic knowledge of metabolism as a guide for our analytical approach with liquid chromatography-mass spectrometry techniques (LC-MS and MS-MS), we here identify the brain and urinary metabolites of PE2I/ $[^{11}\text{C}]\text{PE2I}$  in radiochromatographic (RC) eluates from carrier-added studies. Additionally, we characterize regional brain distribution of radiometabolites by ex vivo measurements to elucidate whether any of them selectively accumulates in striata.

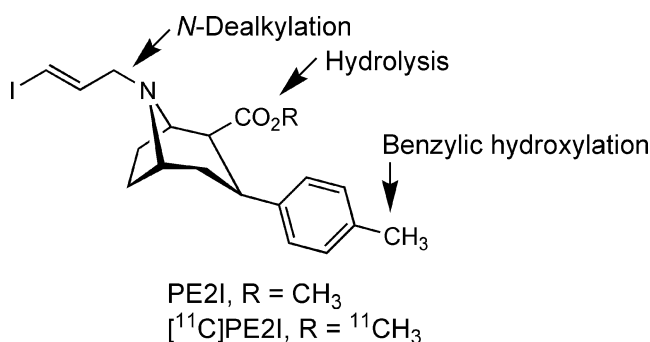


**Fig. 1** Chemical structures and likely biotransformation sites of PE2I and  $[^{11}\text{C}]\text{PE2I}$

## Materials and methods

### Materials

*O*-Desmethyl-PE2I and PE2I [7] were purchased from Pharma Synth AS (Tartu, Estonia). Other materials were obtained from commercial sources and used as received.

### General methods

High-performance liquid chromatography (HPLC) was performed on System Gold apparatus (Beckman Coulter; Fullerton, CA), unless otherwise stated. Radioactivity was measured with a calibrated ionization chamber (Atomlab 300 dose; Biodex Medical Systems; Shirley, NY). cLogD values (for pH 7.4) were calculated from structures with Pallas for Windows 3.0 software (CompuDrug International Inc. South San Francisco, CA).

### Radiosynthesis of $[^{11}\text{C}]\text{PE2I}$

$[^{11}\text{C}]\text{PE2I}$  was prepared by  $^{11}\text{C}$ -methylation of *O*-desmethyl-PE2I with  $[^{11}\text{C}]\text{methyl triflate}$  produced from cyclotron-produced  $[^{11}\text{C}]\text{carbon dioxide}$  via  $[^{11}\text{C}]\text{iodomethane}$  [18].  $[^{11}\text{C}]\text{PE2I}$  was purified with HPLC on an xTerra RP18 column (10  $\mu\text{m}$ ; 7.8 mm $\times$ 250 mm; Waters Corporation, MA) eluted with acetonitrile–10 mM ammonium hydroxide (68:32 v/v; pH 9.7) at 6 ml/min ( $t_R$  of  $[^{11}\text{C}]\text{PE2I}$ , 7.8 min). After removal of mobile phase by evaporation,  $[^{11}\text{C}]\text{PE2I}$  was reconstituted in sterile 0.9% saline (3–5 ml).

HPLC analysis of  $[^{11}\text{C}]\text{PE2I}$  on a Luna C18 column (4.6 mm $\times$ 250 mm; 10  $\mu\text{m}$ ; Phenomenex, Torrance, CA) eluted at 3 ml/min with acetonitrile–10 mM ammonium formate (65:35 v/v), with eluate monitored for absorbance ( $\lambda=230$  nm) and radioactivity, confirmed high chemical and radiochemical purity (>97%). Specific radioactivity was calculated by relating radioactivity ( $[^{11}\text{C}]\text{PE2I}$ ) to the mass associated with the absorbance peak of carrier PE2I. The average specific radioactivity at the end of synthesis was 43.4 GBq/ $\mu\text{mol}$  ( $n=4$ ).

### Animal care and use

Animal experiments were performed in male Sprague-Dawley rats weighing 247–457 g (Taconic, Germantown, NY) in accordance with the *Guide for Care and Use of Laboratory Animals* [26] and were approved by the National Institute of Mental Health (NIMH) Animal Care and Use Committee. Rats were anesthetized with 1.5% isoflurane and 98.5% oxygen inhalation. Anaesthetized rats were placed on a heating pad to maintain body temperature between 36.5° and 37.0°C. Intravenous injections were performed via a cannulated penile vein.

## PET experiment in rat

PET imaging was performed in one rat with an Advanced Technology Laboratory Animal Scanner (ATLAS; NIH). This camera, which is specifically designed for PET imaging in small animals, has a transaxial field of view (FOV) of 6.0 cm and an axial FOV of 2 cm [27]. After anesthesia, the rat was placed in the camera gantry and injected with a bolus of [ $^{11}\text{C}$ ]PE2I (35 MBq; 15.5 GBq/ $\mu\text{mol}$ ; 0.3 ml). Dynamic scan acquisition began at the time of injection and continued for 2 h after injection, with a frame sequence of 20 s $\times$ 6, 60 s $\times$ 5, 120 s $\times$ 4, 300 s $\times$ 3, 600 s $\times$ 3, 1,200 s $\times$ 3. Data were reconstructed in 17 slices by 3D ordered-subset expectation maximization (OSEM) algorithm (3 iterations, 16 subsets) with a final image resolution of 1.6 mm full-width at half-maximum [28, 29]. The reconstructed voxel size was 0.56 $\times$ 0.56 $\times$ 1.12 mm. No attenuation or scatter corrections were applied. All images were decay corrected to the time of injection and analyzed with PMOD (pixel-wise modeling computer software; PMOD Group, Zurich, Switzerland). Regions of interest (ROIs) were drawn on each striatum and the cerebellum with reference to a rat brain stereotaxic atlas [30].

## Biodistribution and composition of no-carrier-added [ $^{11}\text{C}$ ]PE2I radiometabolites in rat plasma and brain tissue

Biodistributions of [ $^{11}\text{C}$ ]PE2I and its radiometabolites were determined ex vivo after injecting three rats with no-carrier-added [ $^{11}\text{C}$ ]PE2I (44.0 $\pm$ 6.1 MBq; 25.0 $\pm$ 5.5 GBq/ $\mu\text{mol}$ ), corresponding to a mass dose of 0.8 $\pm$ 0.1  $\mu\text{g}$  of PE2I equating to 3.0 $\pm$ 0.6  $\mu\text{g/kg}$ . These and subsequent values are expressed as the mean $\pm$ SD.

Thirty minutes after rat injection, a blood sample (2 ml) was drawn by cardiac puncture and then the rat was sacrificed with an intravenous administration of potassium chloride (0.5 mEq/10 ml; Abbott Laboratories, North Chicago, IL). Plasma samples (300  $\mu\text{l}$ ) were separated by centrifugation (Model 426; Thermo IEC, Needham Heights, MA) at 1,800 g for 3 min, placed in acetonitrile (700  $\mu\text{l}$ ) prespiked with PE2I (20  $\mu\text{g}$ ), and mixed. After addition of water (100  $\mu\text{l}$ ), the samples were mixed again.

Regional brain tissues, namely whole cerebellum, striata, and cortex, were dissected out, weighed, and placed in acetonitrile (1–2 ml) containing PE2I (50  $\mu\text{g}$ ) and then counted in a calibrated automatic  $\gamma$ -counter (counting efficiency, 51.9%; model 1480 Wizard; Perkin-Elmer, Boston, MA). Brain tissues were then homogenized (Tissue Tearor; Model 985-370; BioSpec Products Inc.; Bartlesville, OK), with decontamination of the homogenizer between sample treatments. Decontamination was performed by three successive homogenizations in three clean acetonitrile-containing vials to prevent cross-contamination.

All acetonitrile mixtures of plasma and brain tissue samples were counted in a  $\gamma$ -counter followed by centrifugation at 9,400 g for 2 min (Allegra 21R; Beckman Coulter Inc., Palo Alto, CA). Supernates were analyzed by RC (see below).  $\gamma$ -Counter measurements of the precipitates were taken to monitor the acetonitrile extraction efficiency. The radiochemical composition of each tissue was reported as the product of whole tissue counts with their fractional representation in the decay-corrected radiochromatograms. Tissue  $\gamma$ -counts were further normalized to their corresponding tissue weights and decay corrected to the injection time.

The distribution of [ $^{11}\text{C}$ ]PE2I and its radiometabolites in tissues were then expressed as percent standardized uptake values (%SUV) according to the following formula:

$$\frac{\text{activity/tissue}_g}{\text{injected activity}} \times \text{body weight}_g \times 100$$

## In vitro stability of [ $^{11}\text{C}$ ]PE2I in rat brain homogenate and whole blood

Rat whole brain and blood were obtained as mentioned above and placed immediately on ice. The brain was then homogenized in ice-cold 0.9% NaCl (4.5 ml) using a Teflon glass homogenizer (Glas-Col 99C-K54, Terra Haute, IN). Three 1-ml brain homogenate samples and three 0.3-ml blood samples were distributed to six polypropylene test tubes and placed over ice. [ $^{11}\text{C}$ ]PE2I was added to each brain homogenate (23.5 MBq) and blood (12.4 MBq) sample, which were then placed in a 37°C water bath for 1 h. An aliquot (50  $\mu\text{l}$ ) of each sample was removed and placed in acetonitrile (700  $\mu\text{l}$ ) prespiked with authentic PE2I (20  $\mu\text{g}$ ) and analyzed as described above. Each sample (7.4–11.3 kBq) was filtered and injected directly onto the HPLC. The chromatography system permitted the detection of any radiometabolites down to a level of 0.5% of total radioactivity.

## Identification of radiometabolites of [ $^{11}\text{C}$ ]PE2I (carrier-added) in brain and urine

In order to produce sufficient amounts of metabolites for LC-MS analysis, a rat was infused with [ $^{11}\text{C}$ ]PE2I (130 MBq) plus 150  $\mu\text{g}$  of carrier PE2I for 1 h. After sacrifice of the animal, the whole brain was excised and weighed and then the total brain radioactivity was measured. The radioactivity was extracted into acetonitrile, as described above, and analyzed by RC (see below). Guided by the radioactive peaks, chromatographic fractions corresponding to [ $^{11}\text{C}$ ]PE2I and its radiometabolites were separately collected for their identification with LC-MS (see below).

A second rat was infused with PE2I (2.16 mg) alone. Two hours later, urine was surgically withdrawn into a syringe. The rat was then sacrificed by decapitation and the brain excised, homogenized in acetonitrile (4 ml), and centrifuged at 9,400 *g* for 10 min. The clear supernate was saved in a polypropylene tube. The precipitate was rehomogenized with acetonitrile (3 ml) and centrifuged, and the supernates pooled. The urine and brain extracts were stored at  $-70^{\circ}\text{C}$  until LC-MS analysis (see below). Brain, urine, and plasma samples from a rat that was administered only 0.9% NaCl (0.5 ml), and processed as above were used as control samples for the corresponding LC-MS tissue analysis.

#### Radiometabolite analysis with RC

Radiometabolites of [ $^{11}\text{C}$ ]PE2I were analyzed with RC on a Novapak C18 column (100×8 mm; Waters Corp.) contained within a radial compression module (RCM-100) and eluted with mobile phase C (methanol-water-triethylamine; 85:15:0.1 by vol.) at 1.5 ml/min. All biological samples were prefiltered through Nylon filters (13 mm×0.45  $\mu\text{m}$ ; Iso-Disc; Supelco, Bellefonte, PA, USA). The RC system was equipped with an in-line photodiode array detector and a flow-through NaI(Tl) scintillation detector-rate meter (Bioscan; Washington DC). Radiochromatographic data were collected and stored on “Bio-Chrome Lite” software (Bioscan) and analyzed after decay correction. Full recovery of radioactivities after their injection onto the column was confirmed by the absence of eluting radioactivity after the injection of 2 ml of absolute methanol. In a few studies, radioactive ex vivo plasma samples were divided equally. One half was analyzed with the RC system under basic conditions, as described above. The other half was simultaneously analyzed with a HPLC system equipped with a  $\mu$ -Bondapak-C<sub>18</sub> column (3.9×300 mm, Waters Corp.) eluted at 2 ml/min with a gradient acidic mobile phase (50–80% acetonitrile in 10 mM phosphoric acid over 5.5 min).

#### Sample preparation for LC-MS analysis

RC fractions from the carrier-added experiment were concentrated with a SpeedVac evaporator (Thermo Electron Corp.; Milford, MA). Each residue was reconstituted in aqueous methanol (50%; 100  $\mu\text{l}$ ) and transferred to an autosampler vial for LC-MS analysis. Thawed rat urine samples and brain-acetonitrile extracts (diluted with an equal volume of water) were centrifuged (5,000 *g*; 5 min) and the supernates used for LC-MS analysis.

Urine aliquots (100  $\mu\text{l}$ ) were dried azeotropically with acetonitrile (400  $\mu\text{l}$ ) using a SpeedVac evaporator. In order to convert any acid into methyl ester, the residue was

sonicated in acetonitrile (400  $\mu\text{l}$ ) and stirred with 1,1'-carbonyldiimidazole (10 mg) for 1 h before methanol (100  $\mu\text{l}$ ) was added. The reaction mixture was evaporated to dryness. The residue was then dissolved in water (500  $\mu\text{l}$ ) and extracted into ethyl acetate (1 ml) which was then evaporated off. The residue was dissolved in aqueous acetonitrile (50%; 100  $\mu\text{l}$ ) and then analyzed by LC-MS.

#### LC-MS and MS-MS analysis

All urine (2  $\mu\text{l}$ ) and brain (5  $\mu\text{l}$ ) samples were analyzed by LC-MS (LCQ Deca model LC-MS; Thermo Electron Corp.; San Jose, CA) involving reverse-phase HPLC using a Synergi Fusion-RP column (4  $\mu\text{m}$ , 150×2 mm; Phenomenex) that had been pre-equilibrated with 80% mobile phase A (10 mM *aq.* ammonium formate) and 20% mobile phase B [10 mM ammonium formate in acetonitrile-water (90:10 v/v)]. The metabolites were eluted with a linear gradient at 150  $\mu\text{l}/\text{min}$  reaching 20% A and 80% B over 8 min followed by isocratic elution for 6 min. The LC effluents were diverted from waste into the electrospray module of the LC-MS at 2.5 min after the start of analysis runs. At the end of analysis, the mobile-phase composition was returned to 80% A and 20% B over 1 min with a flow rate of 250  $\mu\text{l}/\text{min}$ , allowing column equilibration for 3 min before the start of another analysis.

LC-MS was tuned with a standard solution of PE2I, focusing on the molecular ion  $m/z$  426 generated by electrospray ionization. Electrospray settings were: spray voltage 4.5 kV, sheath gas ( $\text{N}_2$ ) flow rate 50 units, capillary voltage 38 V, and capillary temperature  $260^{\circ}\text{C}$ . In the full scan MS acquisition, the instrument method was set up to detect ions  $m/z$  150 through to 700, a range that encompassed the masses of possible metabolites of PE2I. In MS-MS experiments, the molecular (precursor) ion of PE2I or a metabolite was isolated with 2 amu width and dissociated in the ion trap at a collision energy level of 34%. The energy was adjusted to yield mostly the fragment product ions while retaining a low abundance of the precursor ion.

Control tissue samples were similarly analyzed to confirm the absence of metabolite-specific ions. Verification of chemical structures by MS-MS experiments were performed for each metabolite by comparing the production spectrum with that of PE2I.

## Results

#### PET imaging and time-activity curves

After the intravenous bolus injection of no-carrier-added [ $^{11}\text{C}$ ]PE2I, time-activity curves (TACs) of target DAT-rich



striata and background DAT-devoid cerebellum demonstrated differential washout rates of radioactivity (Fig. 2). Striatal accumulation of radioactivity peaked at 5 min (450% SUV) and was followed by a continuous washout of radioactivity to a level of 210% SUV at 120 min while the cerebellum peaked at 2 min (330% SUV) and declined to a stable level of 38% SUV at 50 min.

PET images of coronal rat brain sections acquired between 30 and 40 min following intravenous bolus administration of [ $^{11}\text{C}$ ]PE2I (Fig. 2, inset) show the typical regional radioactivity distribution. Images display high concentration of radioactivity in the DAT-rich left and right striata and markedly low concentration in the remaining brain regions.

#### RC of plasma and brain metabolites

Acetonitrile efficiently extracted [ $^{11}\text{C}$ ]PE2I and its radiometabolites from plasma and brain regions with recoveries of radioactivity ranging from 93% to 96%. Two radiometabolite peaks, **a** ( $t_R=3.5$  min) and **b** ( $t_R=5.2$  min) along with [ $^{11}\text{C}$ ]PE2I (**c**,  $t_R=6.8$  min) were detected in brain-acetonitrile extracts after 60 min of constant intravenous infusion of carrier-added [ $^{11}\text{C}$ ]PE2I. These peaks represented 21.1%, 16.5%, and 62.4% of the total brain radioactivity, respectively (Fig. 3). A similar RC profile was observed at 30 min after intravenous bolus injection of no-carrier-added [ $^{11}\text{C}$ ]PE2I, where it was  $10.9\pm2.9\%$ ,

$67.1\pm11\%$ , and  $92.5\pm3.2\%$  of the radioactivity present in plasma, cerebellum, and striata, respectively. In each tissue, [ $^{11}\text{C}$ ]PE2I was accompanied by two less lipophilic radiometabolites. RC analysis of urine in one of the animals detected an additional radiometabolite peak that was absent in plasma. Radioactivity was recovered fully from the HPLC column in each analysis. Plasma chromatographic profiles under basic and acidic conditions were quantitatively similar but peaks **a** and **b** switched positions on changing from basic to acidic elution conditions.

#### Regional brain distribution of radiometabolites of [ $^{11}\text{C}$ ]PE2I

Figure 4 shows the distributions of [ $^{11}\text{C}$ ]PE2I and its two radiometabolites, [ $^{11}\text{C}$ ]1 and [ $^{11}\text{C}$ ]2, in plasma, cerebellum, striatum, and cortex. At 30 min following its intravenous injection, [ $^{11}\text{C}$ ]PE2I was  $92.5\pm3.2\%$  of the striatal radioactivity with  $178\pm51\%$  SUV, while in the cerebellum, [ $^{11}\text{C}$ ]PE2I was  $67.1\pm11\%$  of the radioactivity with  $32\pm7\%$  SUV (Fig. 4).

Ratios of concentrations of [ $^{11}\text{C}$ ]PE2I and the two radiometabolites, [ $^{11}\text{C}$ ]1 and [ $^{11}\text{C}$ ]2, in the rat regional brain tissues to their cognates in the cerebellum at 30 min after injection of [ $^{11}\text{C}$ ]PE2I ( $n=3$ ) are presented in Fig. 5. The ratios of the concentrations of the DAT selective probe [ $^{11}\text{C}$ ]PE2I and the radiometabolite [ $^{11}\text{C}$ ]1 in striata to that in the cerebellum were  $6.1\pm3.4$  and  $3.7\pm2.2$ , respectively, and

**Fig. 2** TACs for cerebellum ( $\square$ ), right striatum ( $\blacktriangle$ ) and left striatum ( $\blacktriangledown$ ) after administering no-carrier-added [ $^{11}\text{C}$ ]PE2I (35 MBq) intravenously into one rat. *Inset*: In vivo PET images acquired on the NIH ATLAS, 30–40 min after intravenous injection of [ $^{11}\text{C}$ ]PE2I (35 MBq) into the same rat

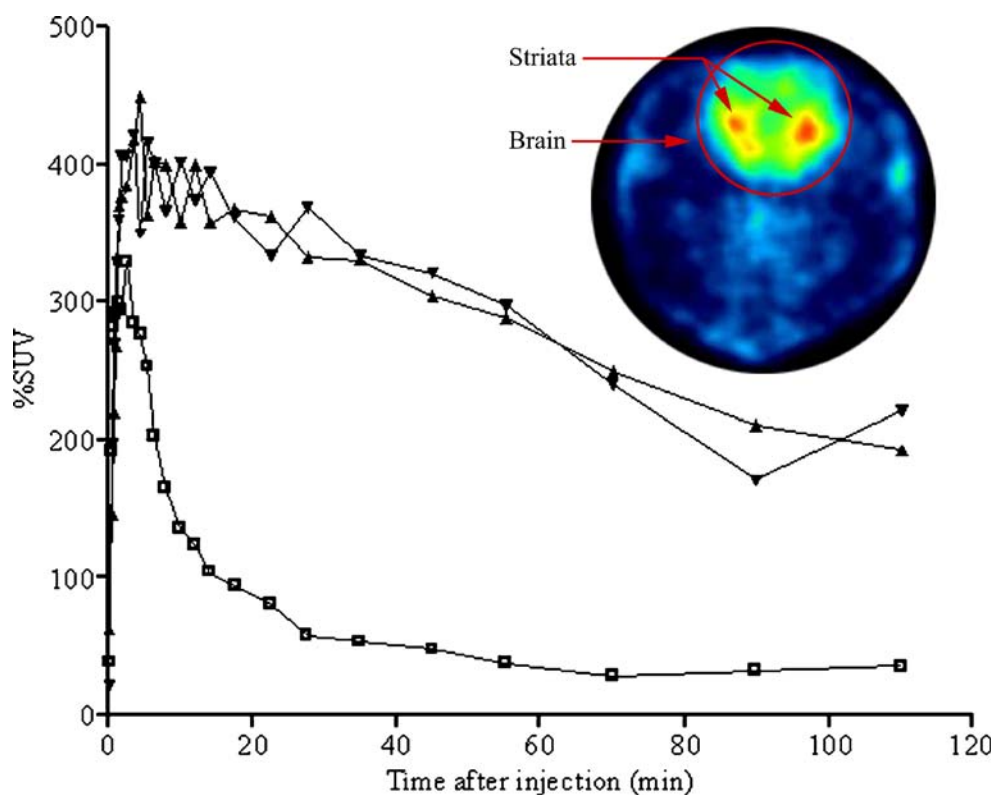
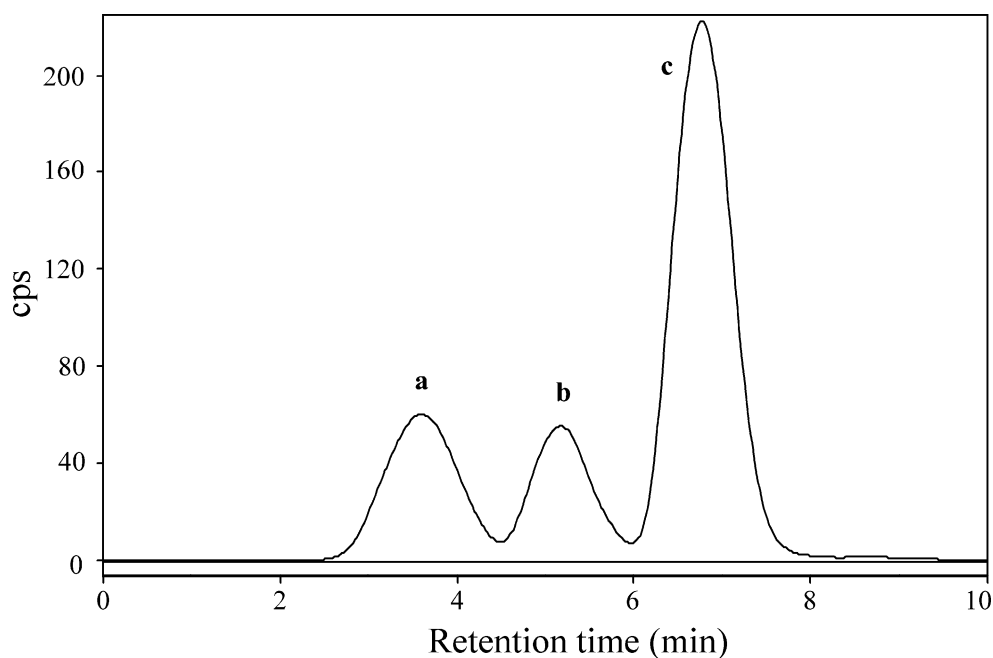


**Fig. 3** Radiochromatogram, obtained under basic conditions, of ex vivo rat brain homogenate 60 min after constant infusion of carrier-added [ $^{11}\text{C}$ ]PE2I (129.5 MBq; 150  $\mu\text{g}$ )



the corresponding ratio for [ $^{11}\text{C}$ ]2 was close to unity ( $1.33 \pm 0.38$ ). Concentrations of both [ $^{11}\text{C}$ ]PE2I and [ $^{11}\text{C}$ ]1 in the brain were higher than those in the plasma while that of [ $^{11}\text{C}$ ]2 was lower in the brain than in plasma (Fig. 5).

In vitro stability of [ $^{11}\text{C}$ ]PE2I in rat brain homogenate and whole blood

The recoveries of radioactivity from in vitro brain samples and blood samples were  $98.7 \pm 0.2\%$  ( $n=3$ ) and  $96.8 \pm 0.5\%$

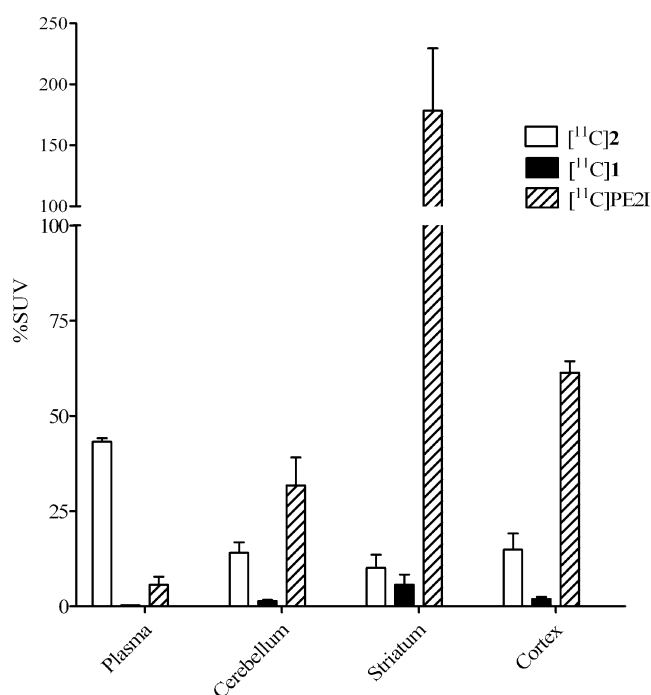


**Fig. 4** Uptake and distribution of [ $^{11}\text{C}$ ]PE2I and its two radiometabolites [ $^{11}\text{C}$ ]1 and [ $^{11}\text{C}$ ]2 in rat brain regions at 30 min after intravenous injection ( $44 \pm 5.9$  MBq;  $n=3$ )

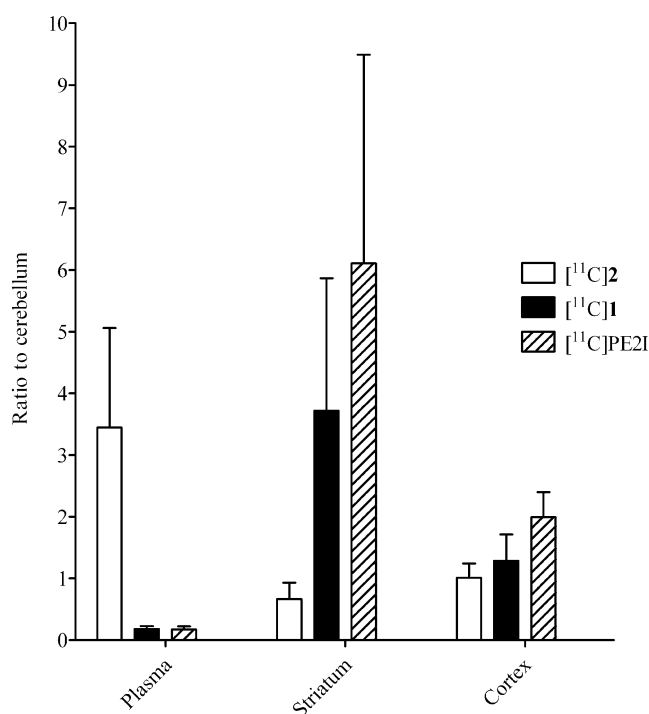


**Fig. 5** Ratios of concentrations of [ $^{11}\text{C}$ ]PE2I and the two radiometabolites, [ $^{11}\text{C}$ ]1 and [ $^{11}\text{C}$ ]2, in rat regional brain tissues to their cognates in cerebellum at 30 min after injection of [ $^{11}\text{C}$ ]PE2I ( $n=3$ )

( $n=3$ ), respectively. [ $^{11}\text{C}$ ]PE2I was stable in rat brain homogenate ( $99.5\pm0.1\%$ ) and in blood ( $99.4\pm0.1\%$ ) after incubation for 1 h at  $37^\circ\text{C}$ .

#### Identification of brain and urinary metabolites of PE2I by LC-MS and MS-MS

Data from the LC-MS and MS-MS analysis of PE2I and its radiometabolites in brain and urine are listed in Table 1. A high correlation ( $r=0.91$ ) was found between the LC retention times and the cLogD values.

Two peaks for metabolites and one peak for PE2I were detected in both brain and urine samples in reconstructed ion-chromatograms between  $m/z$  425 and 457 (Fig. 6). A full scan mass spectrum of peak **c** showed molecular ion  $m/z$  426 for the unmetabolized PE2I in brain and urine. LC-MS analysis of authentic PE2I gave a retention time and mass spectrum identical to those of brain and urine extracts. Brain metabolite peak **b** ( $t_R=9.35$  min) (Fig. 6a) showed molecular ion  $m/z$  442 (Fig. 7, inset) assignable to a hydroxylated PE2I metabolite (**1**), and peak **a** ( $t_R=6.35$  min) exhibited a molecular ion  $m/z$  456 (Table 1) assignable to a carboxylated desmethyl-PE2I metabolite (**2**) (Fig. 8). Similar mass spectra were obtained for peaks **a** and **b** from the analysis of urinary metabolites (Fig. 6b). Extraction of molecular ion alone from the total ion-chromatogram showed only one peak for each of these metabolites in both brain and urine samples. The peak area ratio of metabolite **1** to metabolite **2** was 0.62 for urine and 7.95 for brain samples.

The full scan mass spectrum (inset) and product-ion spectrum (MS-MS) of the precursor ion  $m/z$  442 of metabolite **1** was found in brain and had identical mass spectra to those obtained for the same metabolite peak in the urine (Fig. 7). MS and MS-MS data for PE2I and its other four metabolites are not shown graphically, but

instead the molecular and major fragment ions are listed in Table 1. The prepared methyl ester of **2** showed a single peak ( $t_R=11.1$  min) in the ion-chromatogram for its expected molecular ion  $m/z$  470. Additionally, ions characteristic of the structure of methyl ester **2** were observed in the product-ion spectrum.

LC-MS analysis of urine samples also showed the presence of phase I metabolites resulting from *N*-dealkylation and hydrolysis of PE2I (Fig. 8). The *N*-desalkyl metabolite **3** ( $t_R=9.18$  min) showed the expected molecular ion  $m/z$  260. The molecular ion  $m/z$  412 for the acid metabolite **5** was found at  $t_R=7.87$  min in the total-ion chromatogram. It was a minor product that constituted 1.5% of the total-ion current of all metabolites combined. Another secondary metabolite, **4**, the product of both *N*-dealkylation and aryl methyl group hydroxylation, was detected in urine ( $t_R=5.46$  min;  $m/z$  276). In RC and LC-MS, these urinary metabolites appear minor. LC-MS analysis did not detect **3–5** in the brain.

#### Discussion

After intravenous administration of [ $^{11}\text{C}$ ]PE2I into rat, clear images of DAT-rich striata were obtained between 30 and 40 min after injection (Fig. 2, inset), as expected. The corresponding TAC for striata showed high initial uptake of radioactivity followed by a slow continuous decline until the end of the experiment (Fig. 2). DAT-devoid cerebellum also had a high initial uptake of radioactivity, which was followed by fast washout up to 55 min after radioligand injection. However, the concentration of radioactivity in cerebellum was maintained to the end of the experiment (Fig. 2). The difference in regional radioactivity kinetics suggested the possibility of a retention or accumulation of one or more radiometabolites in cerebellum. Arguably, such radiometabolites may exhibit selectivity for binding to DAT, or may distribute nonspecifically across all brain regions. Their presence in rat brain would potentially compromise the use of [ $^{11}\text{C}$ ]PE2I to measure DAT.

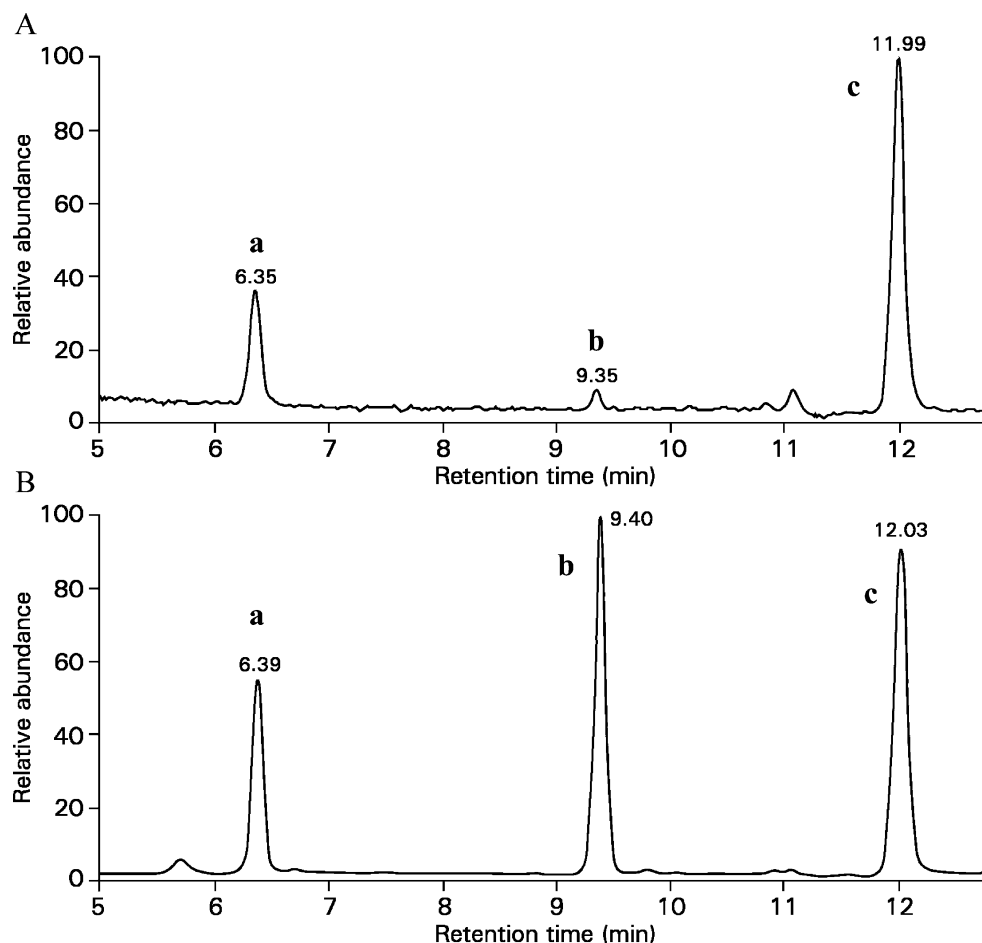
Radiochromatographic analysis of the plasma extract (>90% radioactivity recovered) showed two distinct peaks for radiometabolites in addition to [ $^{11}\text{C}$ ]PE2I. Each of the two radiometabolites was less lipophilic than [ $^{11}\text{C}$ ]PE2I. A similar pattern of radiometabolites has been observed in HPLC analyses of plasma after administration of [ $^{11}\text{C}$ ]PE2I to human subjects [18] which were run under acidic conditions. In our study, direct comparison of radiochromatograms obtained under basic elution conditions with those obtained under acidic conditions showed similar proportions of parent radioligand and its radiometabolites in plasma, but with the two detected radiometabolites in switched order of elution. This indicates that one of the

**Table 1** cLogD, LC-MS, and MS-MS data for PE2I and its metabolites. The metabolites are listed in the descending order of LC retention times

Compound	cLogD	LC retention time (min)	Molecular ion ( $m/z$ )	Major fragment ions ( $m/z$ )
PE2I	4.02	12.0	426	394, 366, 276, 240
<b>1</b>	2.70	9.40	442	424, 410, 392, 382, 314, 276
<b>3</b>	0.77	9.18	260	228
<b>5</b>	0.09	7.87	412	394, 366, 276, 240
<b>2</b>	0.16	6.39	456	424, 406, 396, 328, 296
<b>4</b>	-0.43	5.46	276	258, 244, 226



**Fig. 6** Partial ion-chromatogram ( $m/z$  425, 457) with peaks of PE2I and its major metabolites in brain (a) and urine (b). Peaks a and b were identified as metabolites 2 and 1, respectively, and peak c as PE2I



radiometabolites is acidic. Therefore, we hypothesized that the acidic radiometabolite is the phenyl carboxylic acid (2). The radiochromatographic profile of ex vivo brain extract (Fig. 3) was found to be qualitatively similar to that of plasma. The presence of these radiometabolites in rat brain

accords with the observed differences in rate of washout of radioactivities between brain regions. Since our experiments showed that [ $^{11}\text{C}$ ]PE2I is stable in rat brain homogenates, we can deduce that the detected brain radiometabolites have peripheral origin.

**Fig. 7** Electrospray mass spectrum (inset) and product-ion spectrum of metabolite 1 (peak b in Fig. 6a) in the brain

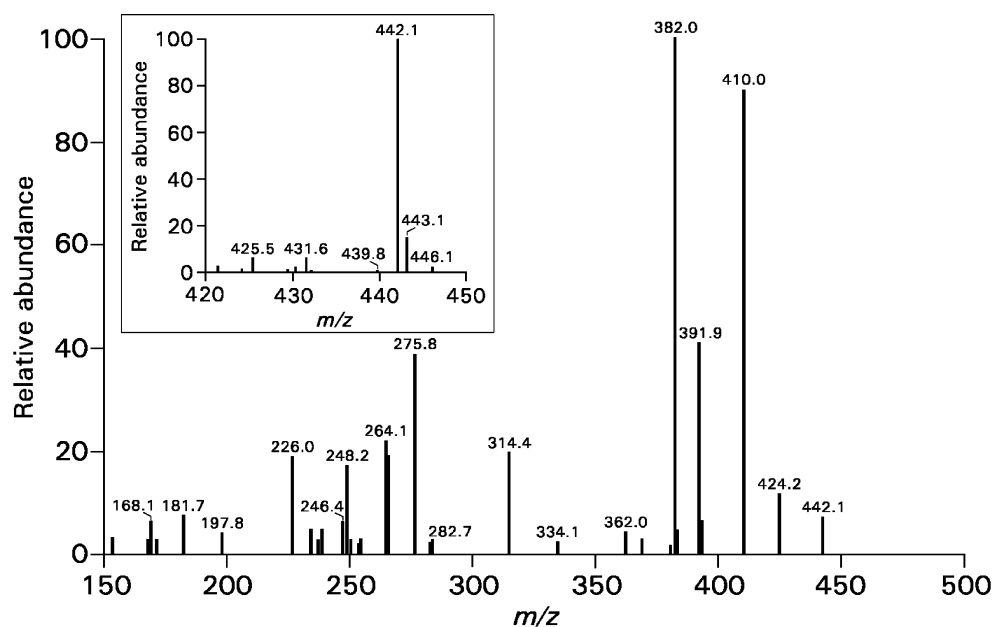
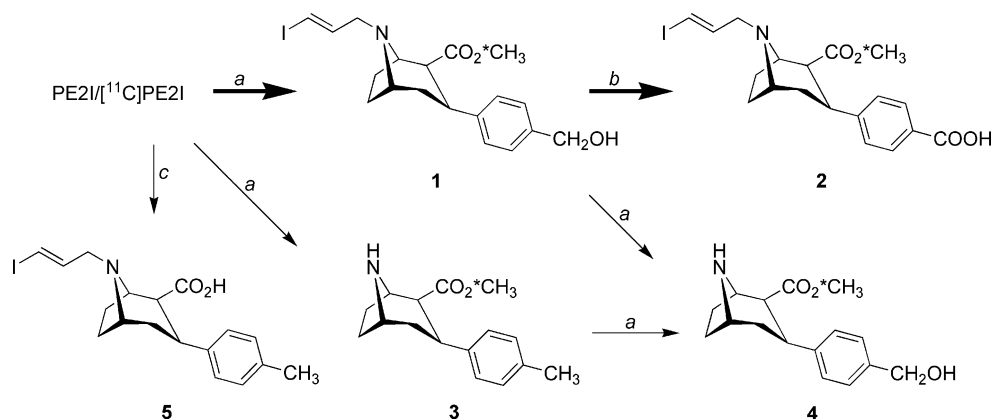


**Fig. 8** Proposed structures and genesis of PE2I metabolites in brain (**1**, **2**) and urine (**1**–**5**) through (a) cytochrome P450, (b) alcohol, and aldehyde dehydrogenases and (c) esterase. An asterisk indicates the position of the  $^{11}\text{C}$  label



The biodistributions of  $[^{11}\text{C}]$ PE2I and its two radiometabolites were examined in striata, cerebellum, and cortex. As expected at 30 min after radioligand injection, the concentration of  $[^{11}\text{C}]$ PE2I was severalfold higher in striata than in DAT-poor cortex or DAT-devoid cerebellum (Fig. 4). The two radiometabolites,  $[^{11}\text{C}]$ **1** and  $[^{11}\text{C}]$ **2**, were found in all three examined regions at lower concentrations than  $[^{11}\text{C}]$ PE2I. In order to identify a possible selective striatal uptake of  $[^{11}\text{C}]$ **1** or  $[^{11}\text{C}]$ **2**, the concentration (%SUV) of each compound in each brain region was divided by its corresponding concentration in cerebellum, giving ratios of  $6.1 \pm 3.4$  for  $[^{11}\text{C}]$ PE2I and  $3.7 \pm 2.2$  for the radiometabolite  $[^{11}\text{C}]$ **1**. This analysis (Fig. 5) revealed that  $[^{11}\text{C}]$ **1** is selectively taken up by striata. It therefore seems probable that  $[^{11}\text{C}]$ **1**, given its derivation from  $[^{11}\text{C}]$ PE2I, has high affinity for DAT, but  $[^{11}\text{C}]$ **2** with similar brain regional concentration to that in the cerebellum does not. The higher concentrations of  $[^{11}\text{C}]$ PE2I and  $[^{11}\text{C}]$ **1** in brain than in the plasma indicate significant brain uptake and retention.

We aimed to identify  $[^{11}\text{C}]$ **1** and  $[^{11}\text{C}]$ **2** to better understand the metabolism of  $[^{11}\text{C}]$ PE2I. Following its systemic administration, PE2I is expected to undergo phase I biotransformations, such as *N*-dealkylation and benzylic hydroxylation (Fig. 1) by cytochrome P450 enzymes, predominantly in the liver [22–25]. Also, secondary metabolites may result from a combination of these actions and further oxidation of the benzyl alcohol metabolite. Besides the action of cytochrome P450, a nonspecific esterase is expected to hydrolyze the ester group and generate the carboxylic acid metabolite of PE2I.

To identify all possible radiometabolites of PE2I in brain and periphery, two animal experiments were performed. In one experiment, a high dose of PE2I alone was infused into the rat to obtain a good yield of corresponding nonradioactive metabolites in brain and urine. This experiment aimed to generate all significant metabolites in sufficient amounts for LC-MS detection. Most of the plasma metabolites are expected to be excreted by the kidney and

concentrated in the urine [24]. Thus, urine was collected for the entire duration of PE2I infusion and used for metabolite identification. In contrast to plasma, it was possible to inject the clear urine sample directly into LC-MS, eliminating the need for protein precipitation, concentration, or any other sample preparation step. Once the major metabolites of PE2I had been identified in brain and urine, we aimed to identify the nonradioactive metabolites co-eluting with radiometabolites of  $[^{11}\text{C}]$ PE2I on HPLC. Thus, in another experiment a significant quantity of PE2I was injected along with  $[^{11}\text{C}]$ PE2I into rat to allow identification of the co-eluting radiometabolites with LC-MS techniques.

LC-MS generated molecular ion  $m/z$  426 for PE2I whereas the metabolite **1** generated molecular ion  $m/z$  442 (Table 1), an increase of 16 mass units, consistent with hydroxylation of PE2I to **1**. MS-MS generated characteristic product ions for PE2I, such as  $m/z$  394 and 366 (Table 1), owing to loss of the neutral species  $\text{CH}_3\text{OH}$  and  $\text{HCOOCH}_3$ , respectively. Analogous fragmentation of the molecular ion  $m/z$  442 of metabolite **1** generated product ions  $m/z$  410 and 382 (Fig. 7), both ions showing an increment of 16 mass units, consistent with the presence of a hydroxyl group in the parent molecule and retention of this group in each of the fragment ions. Unlike the production spectrum of PE2I, that of metabolite **1** showed a fragment ion  $m/z$  424 owing to loss of  $\text{H}_2\text{O}$  from the parent ion  $m/z$  442. This transition is characteristic of benzylic cleavage of a hydroxyl group, an energetically favorable process leading to the formation of a resonance-stabilized benzyl cation that may subsequently rearrange into a tropylium ion [31, 32]. Formation of fragment ion  $m/z$  424 rules out the presence of a hydroxyl group on the aromatic ring. Also, consistent with its benzyl alcohol structure, a similar fragmentation was observed for the molecular ion  $m/z$  276 of the secondary amine **4**, a metabolite derived from the secondary amine metabolite **3** by hydroxylation or the metabolite **1** by *N*-dealkylation (Fig. 8).

A benzylic carbon (methyl or methylene) is highly prone to hydroxylation by drug-metabolizing cytochrome P450

enzymes. This biotransformation has been amply demonstrated in drugs and aromatic hydrocarbons. Some examples of drugs that undergo benzylic hydroxylation are tolbutamide [33], metoprolol [34], and tolterodine [35]. Also, toluene, the simplest benzylic system, is metabolized predominantly into benzyl alcohol by cytochrome P450 [36, 37]. Thus, it is very probable that liver cytochrome P450 enzymes are responsible for the formation of the identified hydroxylated metabolite **1** from PE2I.

Another major metabolite, **2**, found in both plasma and brain, was identified as a carboxylic acid derivative of PE2I. The mass spectral data, molecular ion, and fragment ions are consistent with the benzoic acid structure proposed here for this metabolite (Fig. 8). Conversion of this metabolite into the methyl ester gave a molecular ion at the expected mass (data not shown). Its MS-MS data were also consistent with the structure of the proposed methyl ester of metabolite **2**. The structure proposed for metabolite **2** is also supported by our detection and identification of its obligatory precursor metabolite, **1**, a primary alcohol that is likely to be readily oxidized to the aldehyde by cytochrome P450 [36] or alcohol dehydrogenase [38]. The generated aldehyde would be expected to be transient owing to fast conversion into the benzoic acid **2** by an aldehyde dehydrogenase [39]. Such a sequential biotransformation of a benzylic group into carboxylic acid has been well characterized [33, 35, 37].

The brain and urinary metabolites, **1** and **2**, identified following administration of PE2I, correspond to the two major radiometabolites found in plasma and rat brain following the administration of [ $^{11}\text{C}$ ]PE2I. Metabolite **1** (cLogD at pH 7.4=2.70; Table 1) is likely to cross the blood-brain barrier from plasma. However, it is unlikely that a significant amount of the more polar metabolite **2**, which is predominantly ionic at physiological pH (cLogD at pH 7.4=0.16; Table 1), readily enters brain from plasma [40, 41]. Although cytochrome P450 enzymes are not highly expressed in brain [42], alcohol and aldehyde dehydrogenases are present [43, 44] and might oxidize **1** into the benzoic acid **2**. Peak area measurements (in the carrier-alone experiment) show that the ratio of **2** to **1** in brain is several times higher than in urine, a finding consistent with conversion of **1** into **2** within brain. Conversely, however, contribution of a transporter-mediated entry of acid metabolite **2** into brain may not be ruled out. Apart from the two metabolites from oxidation of the aryl methyl group in PE2I, LC-MS analysis showed no detectable levels of metabolites **3–5** in the brain. Thus, the radiolabeled analogs of **3** and **4** are unlikely to contribute to rat brain radioactivity when [ $^{11}\text{C}$ ]PE2I is administered. However, the minor acid metabolite **5** detected in the urine would have necessarily been accompanied with an equivalent amount of [ $^{11}\text{C}$ ]methanol. Should oxidative metabo-

lism of [ $^{11}\text{C}$ ]methanol take place subsequently, only a low level of [ $^{11}\text{C}$ ]carbon dioxide would be generated.

Notably, the reverse phase HPLC retention times (mobile phase, pH 7.0) for the PE2I metabolites correlated well ( $r=0.91$ ) with their cLogD values (at pH 7.4) calculated from their identified structures (Table 1). Hence, these data are fully consistent with the deduced identities of the metabolites **1–5**.

The utility of [ $^{11}\text{C}$ ]PE2I in quantifying DAT in human brain has been assessed recently [19]. Human plasma showed two radiometabolites, less lipophilic than [ $^{11}\text{C}$ ]PE2I, as in the rodent. Binding potential values in human striatum obtained by compartmental analyses were about 30% higher than those obtained with a reference tissue model. These discrepant values might also be attributed to the presence of radiometabolites in human brain, among other possible causes [19].

## Conclusion

Radiometabolites [ $^{11}\text{C}$ ]**1** and [ $^{11}\text{C}$ ]**2** are the 4-hydroxymethyl and 4-carboxyl analogs of [ $^{11}\text{C}$ ]PE2I. [ $^{11}\text{C}$ ]**1**, detected in plasma, appears to selectively accumulate in striata, presumably by binding to DAT. This bioactive metabolite is probably transformed within brain into the inactive acid metabolite [ $^{11}\text{C}$ ]**2**. These findings limit the utility of [ $^{11}\text{C}$ ]PE2I for measuring DAT in rat brain with PET.

**Acknowledgement** This work was supported by the Intramural Research Program of NIH (NIMH; project no. Z01-MH002795-04).

## References

1. Nurmi E, Ruottinen HM, Kaasinen V, Bergman J, Haaparanta M, Solin O, et al. Progression in Parkinson's disease: a positron emission tomography study with a dopamine transporter ligand [ $^{18}\text{F}$ ]CFT. *Ann Neurol* 2000;47:804–8.
2. Seibyl JP, Marek KL, Quinlan D, Sheff K, Zoghbi S, Zea-Ponce Y, et al. Decreased SPECT [ $^{123}\text{I}$ ]β-CIT striatal uptake correlates with symptom severity in Parkinson's disease. *Ann Neurol* 1995;38:589–98.
3. Innis RB, Seibyl JP, Scanley BE, Laruelle M, Abi-Dargham A, Wallace E, et al. Single photon emission computed tomographic imaging demonstrates loss of striatal dopamine transporters in Parkinson disease. *Proc Natl Acad Sci U S A* 1993;90:11965–9.
4. Meyer JH, Krüger S, Wilson AA, Christensen BK, Goulding VS, Schaffer A, et al. Lower dopamine transporter binding potential in striatum during depression. *NeuroReport* 2001;12:4121–5.
5. Laakso A, Bergman J, Haaparanta M, Vilkmann H, Solin O, Syvälahti E, et al. Decreased striatal dopamine transporter binding in vivo in chronic schizophrenia. *Schizophr Res* 2001;52:115–20.
6. Malison RT, McDougle CJ, van Dyck CH, Scahill L, Baldwin RM, Seibyl JP, et al. [ $^{123}\text{I}$ ]β-CIT SPECT imaging of striatal dopamine transporter binding in Tourette's disorder. *Am J Psychiatry* 1995;152:1359–61.

7. Emond P, Garreau L, Chalon S, Boazi M, Caillet M, Bricard J, et al. Synthesis and ligand binding of nortropine derivatives: *N*-substituted 2 $\beta$ -crabomethoxy-3 $\beta$ -(4'-iodophenyl)nortropine and *N*-(3-iodoprop-(2*E*)-enyl)-2 $\beta$ -carbomethoxy-3 $\beta$ -(3',4'-disubstituted phenyl)nortropine. New high-affinity and selective compounds for the dopamine transporter. *J Med Chem* 1997;40: 1366–72.
8. Guilloteau D, Emond P, Baulieu J-L, Garreau L, Frangin Y, Pourcelot L, et al. Exploration of the dopamine transporter: in vitro and in vivo characterization of a high-affinity and high-specificity iodinated tropane derivative (*E*)-*N*-(3-iodoprop-2-enyl)-2 $\beta$ -carbomethoxy-3 $\beta$ -(4'-methylphenyl)nortropine (PE2I). *Nucl Med Biol* 1998;25:331–7.
9. Goodman MM, Keil R, Shoup TM, Eshima D, Eshima L, Kilts C, et al. Fluorine-18-FPCT: a PET radiotracer for imaging dopamine transporters. *J Nucl Med* 1997;38:119–26.
10. Goodman MM, Kilts CD, Keil R, Shi B, Martarello L, Xing D, et al. [<sup>18</sup>F]-labeled FECNT: a selective radioligand for PET imaging of brain dopamine transporters. *Nucl Med Biol* 2000;27:1–12.
11. Goodman MM, Kung M-P, Kabalka GW, Kung HF, Switzer R. Synthesis and characterization of radioiodinated *N*-(3-iodoprop-1-yl)-2 $\beta$ -carbomethoxy-3 $\beta$ -(4-chlorophenyl)tropanes: potential dopamine reuptake site imaging agents. *J Med Chem* 1994;37: 1535–42.
12. Xing D, Chen P, Keil R, Kilts CD, Shi B, Camp VM, et al. Synthesis, biodistribution, and primate imaging of fluorine-18 labeled 2 $\beta$ -carbo-1'-fluoro-2-propoxy-3 $\beta$ -(4-chlorophenyl)tropanes. Ligands for the imaging of dopamine transporters by positron emission tomography. *J Med Chem* 2000;43:639–48.
13. Neumeyer JL, Wang S, Gao Y, Milius RA, Kula NS, Campbell A, et al. *N*- $\omega$ -Fluoroalkyl analogs of (1*R*)-2 $\beta$ -carbomethoxy-3 $\beta$ -(4-iodophenyl)tropane ( $\beta$ -CIT): radiotracers for positron emission tomography and single photon emission computed tomography imaging of dopamine transporters. *J Med Chem* 1994;37:1558–61.
14. Davis MR, Votaw JR, Bremner JD, Byas-Smith MG, Faber TL, Voll RJ, et al. Initial human PET imaging studies with the dopamine transporter ligand <sup>18</sup>F-FECNT. *J Nucl Med* 2003;44:855–61.
15. Lu J-Q, Rodrigues-Gomez JA, Velasco I, Zoghbi SS, Liow J-S, Musachio JL, et al. PET imaging of DAT with [<sup>18</sup>F]FECNT in naive and Parkinsonian rats following embryonic stem cell transplantation [abstract]. *NeuroImage* 2004;22:T27–T28.
16. Zoghbi SS, Shetty HU, Ichise M, Fujita M, Imaizumi M, Liow J-S, et al. PET imaging of the dopamine transporter with <sup>18</sup>F-2 $\beta$ -carbomethoxy-3 $\beta$ -(4-chlorophenyl)-8-(2-fluoroethyl)nortropine: a polar radiometabolite confounds brain radioligand measurements. *J Nucl Med* 2006;47:520–7.
17. Kuikka JK, Baulieu JL, Hiltunen J, Halldin C, Bergström K, Farde L, et al. Pharmacokinetics and dosimetry of iodine-123 labelled PE2I in humans, a radioligand for dopamine transporter imaging. *Eur J Nucl Med* 1998;25:531–4.
18. Halldin C, Erixon-Lindroth N, Pauli S, Chou Y-H, Okubo Y, Karlsson P, et al. [<sup>11</sup>C]PE2I: a highly selective radioligand for PET examination of the dopamine transporter in monkey and human brain. *Eur J Nucl Med Mol Imaging* 2003;30:1220–30.
19. Jucaite A, Odano I, Olsson H, Pauli S, Halldin C, Farde L. Quantitative analyses of regional [<sup>11</sup>C]PE2I binding to the dopamine transporter in the human brain: a PET study. *Eur J Nucl Med Mol Imaging* 2006;33:657–68.
20. Jucaite A, Fernell E, Halldin C, Forssberg H, Farde L. Reduced midbrain dopamine transporter binding in male adolescents with attention-deficit/hyperactivity disorder: association between striatal dopamine markers and motor hyperactivity. *Biol Psychiatry* 2005;57:229–38.
21. Zoghbi SS, Shetty UH, Ichise M, Hong J, Musachio JL, Seneca N, et al. The dopamine transporter probe [<sup>11</sup>C]PE2I shows active and inactive radioactive metabolites in rat brain [abstract]. *J Label Compds Radiopharm* 2005;48 Suppl 1: S98.
22. Hawkins DR, editor. Biotransformations: a survey of the biotransformations of drugs and chemicals in animals. Cambridge: The Royal Society of Chemistry; 1992.
23. Jenner P, Testa B, editors. Concepts in drug metabolism. New York: Marcel Dekker, Inc.; 1980.
24. Woolf TF, editor. Handbook of drug metabolism. New York: Marcel Dekker, Inc.; 1999.
25. Guengerich FP. Common and uncommon cytochrome P450 reactions related to metabolism and chemical toxicity. *Chem Res Toxicol* 2001;14:611–50.
26. Clark JD, Baldwin RL, Bayne KA, Brown MJ, Gebhart GF, Gonder JC, et al. Guide for the care and use of laboratory animals. Washington, DC: National Academy Press; 1996.
27. Seidel J, Vaquero JJ, Green MV. Resolution uniformity and sensitivity of the NIH ATLAS small animal PET scanner: comparison to simulated LSO scanners without depth-of-interaction capability. *IEEE Trans Nucl Sci* 2003;50:1347–50.
28. Johnson CA, Seidel J, Vaquero JJ, Pascau J, Desco M, Green MV. Exact positioning for OSEM reconstructions on the ATLAS depth-of-interaction small animal scanner [abstract]. *Mol Imaging Biol* 2002;4:S22.
29. Liow JS, Johnson CA, Toyama H, Green MV, Innis RB. A single slice rebinning/2D exact positioning OSEM reconstruction for the NIH ATLAS small animal PET scanner [abstract]. *J Nucl Med* 2003;44 Suppl:P163.
30. George P, Watson C. The rat brain in stereotaxic coordinates. 4th ed. San Diego: Academic Press; 1998.
31. McLafferty FW, Tureček F. Interpretation of mass spectra. 4th ed. Mill Valley: University Science Books; 1993.
32. Tozuka Z, Kaneko H, Shiraga T, Mitani Y, Beppu M, Terashita S, et al. Strategy for structural elucidation of drugs and drug metabolites using (MS)<sup>n</sup> fragmentation in an electrospray ion trap. *J Mass Spectrom* 2003;38:793–808.
33. Thomas RC, Ikeda GJ. The metabolic fate of tolbutamide in man and in the rat. *J Med Chem* 1966;9:507–10.
34. Shetty HU, Nelson WL. Chemical aspects of metoprolol metabolism. Asymmetric synthesis and absolute configuration of the 3-[4-(1-hydroxy-2-methoxyethyl)phenoxy]-1-(isopropylamino)-2-propanols, the diastereomeric benzylic hydroxylation metabolites. *J Med Chem* 1988;31:55–9.
35. Andersson SHG, Lindgren A, Postlind H. Biotransformation of tolterodine, a new muscarinic receptor antagonist, in mice, rats and dogs. *Drug Metab Disp* 1998;26:528–35.
36. Hanioka H, Hamamura M, Kakino K, Ogata H, Jinno H, Takahashi A, et al. Dog liver microsomal P450 enzyme-mediated toluene biotransformation. *Xenobiotica* 1995;25:1207–17.
37. Chapman DE, Moore TJ, Michener SR, Powis G. Metabolism and covalent binding of [<sup>14</sup>C]toluene by human and rat liver microsomal fractions and liver slices. *Drug Metab Disp* 1990;18:929–36.
38. Wagner FW, Burger AR, Vallee BL. Kinetic properties of human liver alcohol dehydrogenase: oxidation of alcohols by class I isoenzymes. *Biochemistry* 1983;22:1857–63.
39. Lindahl R, Evces S. Rat liver aldehyde dehydrogenase I. Isolation and characterization of four high *K<sub>m</sub>* normal liver isozymes. *J Biol Chem* 1984;259:11986–90.
40. Rapoport SI, Ohno K, Pettigrew KD. Drug entry into the brain. *Brain Res* 1979;172:354–9.
41. Pardridge WM. CNS drug design based on principles of blood-brain barrier transport. *J Neurochem* 1998;70:1781–92.

42. Anandatheerthavarada HK, Boyd MR, Ravindranath V. Characterization of a phenobarbital-inducible cytochrome *P*-450, NADPH-cytochrome *P*-450 reductase and reconstituted cytochrome *P*-450 mono-oxygenase system from rat brain: evidence for constitutive presence in rat and human brain. *Biochem J* 1992;288:483–8.
43. Galter D, Carmine A, Buervenich S, Duester G, Olson L. Distribution of class I, III and IV alcohol dehydrogenase mRNAs in the adult rat, mouse and human brain. *Eur J Biochem* 2003;270:1316–26.
44. Erwin VG, Deitrich RA. Brain aldehyde dehydrogenase: localization, purification, and properties. *J Biol Chem* 1966;241:3533–9.